HHS Public Access

Author manuscript

Nat Chem. Author manuscript; available in PMC 2018 March 01.

Published in final edited form as:

Nat Chem. 2017 March ; 9(3): 257–263. doi:10.1038/nchem.2643.

Why copper is preferred over iron for oxygen activation and reduction in heme-copper oxidases

Ambika Bhagi-Damodaran[†], **Matthew A. Michael**[‡], **Qianhong Zhu**[#], **Julian Reed**[§], **Braddock A. Sandoval**[†], **Evan N. Mirts**[‖], **Saumen Chakraborty**[†], **Pierre Moënne-Loccoz**[#,*], **Yong Zhang**[‡,*], and **Yi Lu**[†,§,‖,*]

[†]Department of Chemistry, University of Illinois at Urbana-Champaign, Urbana, IL, USA

[§]Department of Biochemistry, University of Illinois at Urbana-Champaign, Urbana, IL, USA

[‖]Center for Biophysics and Quantitative Biology, University of Illinois at Urbana-Champaign, Urbana, IL, USA

[‡]Department of Biomedical Engineering, Chemistry, and Biological Sciences, Stevens Institute of Technology, Hoboken, NJ, USA

[#]Division of Environmental & Biomolecular Systems, Institute of Environmental Health, Oregon Health & Science University, 3181 SW Sam Jackson Park Road, Portland, OR, USA

Abstract

Heme-copper oxidase (HCO) catalyzes the natural reduction of oxygen to water using a heme-copper center. Despite decades of research on HCO's, the role of nonheme metal and Nature's choice of copper over other metals like iron remains unclear. Here, we use a biosynthetic model of HCO in myoglobin that selectively binds different nonheme metals to demonstrate 30-fold and 11-fold enhancements in oxidase activity of Cu- and Fe-bound HCO mimics respectively, as compared to Zn-bound mimics. Detailed electrochemical, kinetic and vibrational spectroscopic studies, in tandem with theoretical DFT calculations demonstrate that the nonheme metal not only donates electrons to oxygen but also activates it for efficient O-O bond cleavage. Furthermore, the higher redox potential of copper and the enhanced weakening of O-O bond from the higher electron density in the *d*-orbital of copper are central to its higher oxidase activity over iron. This work resolves a long-standing question in bioenergetics, and renders a chemical-biological basis for designing future oxygen reduction catalysts.

Heme-Copper Oxidases (HCOs) are terminal oxidases involved in aerobic respiration in many forms of lives from bacteria to eukaryotes and human. They contain a heterobinuclear heme-copper center which is responsible for catalyzing the four-electron reduction of oxygen to water, and transforming the chemical energy into ATP, which is then utilized as an energy currency for many cellular processes.[1–3] The HCO superfamily consists of two sets

[*]Corresponding author yi-lu@illinois.edu; yong.zhang@stevens.edu; moennelo@ohsu.edu.

Author contributions: A.B.D. and Y.L. designed research; A.B.D., J.R. and B.A.S. purified and characterized protein, performed oxygen reduction assays, electrochemical, EPR and stopped-flow experiments, E.M. performed XANES study and analyzed data, S.C. helped with initial assay design, M. A. M. and Y.Z. performed DFT calculations, Q.Z. and P.M.L. performed RR experiments. A.B.D. Y.Z., P.M.L. and Y.L. wrote the paper. All authors contributed in developing the rationale of the manuscript and analysis of results.

of homologous enzymes with significant sequence and structural homology: the heme-copper oxidases that contain a heme and a copper in the nonheme site (referred to as HCO in this work) and nitric oxide reductases (NORs) that contains a heme and an iron in the nonheme site (Supplementary Fig. S1). The HCOs perform four-electron reduction of O_2 to water, while NORs carry out the two-electron reduction of NO to N_2O.[4–5] Several phylogenetic studies have suggested that HCOs and NORs have evolved from a common ancestral protein by "tinkering" of its catalytic center to select a copper for HCOs and a nonheme iron for NORs.[6–8] While some NORs exhibit HCO reactivity, *i.e.* reduce O_2 to H_2O, they do so with rates significantly lower than that of HCOs.[9] The high structural homology and similar active site of HCOs and NORs raises a fundamental question as to why copper is preferred over iron for oxygen reduction in HCOs.[10] While deterministic experimental routes to probe such a preference has been inaccessible till date, even questions of a broader nature such as the function of the nonheme metal towards oxidase activity has remained controversial.[4,11]

One approach to answer these questions would be to replace the copper in native HCOs with iron, followed by investigations of its effect on the electronic structure of the binuclear center and on the formation of O_2 reaction intermediates, all of which can impact oxidase activity. However, despite much effort it has not been possible to extract the copper out of HCOs and add iron back in without disrupting the structure and destroying the activity of the enzyme. This difficulty arises from challenges of working with large (MW ~100–200 KDa) membrane proteins like HCOs, which also contain other metal centers. To overcome these limitations with studying complex metalloproteins like HCOs, synthetic models of HCOs using organic molecules have been prepared.[12–14] In particular, using small-molecule HCO models, Collman *et. al.* showed that both copper and iron at the nonheme center could selectively reduce oxygen to water,[15] however, the difference in their reaction rates and reason for preference of copper in HCOs was not explored. As an alternative approach to studying complex native enzymes or small synthetic models, biosynthetic modeling, that uses smaller proteins and peptides, combines the advantages of simpler system of synthetic models while retaining many structural features of native enzymes.[16–22] Using this approach, we have designed structural and functional models of the active site of HCOs and NORs in small (MW ~ 17.4 KDa), easy-to-purify, and water-soluble protein myoglobin, called Cu_BMb and Fe_BMb, respectively.[23–24] In this study, we focus on Fe_BMb that can be purified as heme-containing protein with the nonheme center unoccupied. By titrating Cu^I, Fe^{II}, or a control redox-inactive Zn^{II} metal ions into the nonheme metal center, we herein report the first systematic investigation of the role of the nonheme metal ion in HCO activity and demonstrate why copper is preferred over iron.

Results and discussion

The Fe_BMb refers to Mb mutant protein in which a nonheme Fe_B site containing 3-His, 1-Glu residues found in native NORs has been engineered into Mb. Unlike native NORs, the Fe_BMb protein could be purified without any metal ion at the nonheme Fe_B center and is referred to as empty-$Fe_BMb(Fe^{II})$ or simply E-$Fe_BMb(Fe^{II})$ where Fe^{II} in parenthesis represents the heme iron in +2 oxidation state. When the Fe_B center is occupied by a metal ion, they are called M^{II}-$Fe_BMb(Fe^{II})$ where M^{II} represents the metal ion with the designated

oxidation state that occupies the nonheme Fe_B center. We first expressed and purified E-Fe_BMb using a protocol reported previously,[24–26] and then titrated Zn^{II}, Fe^{II} or Cu^{I} into E-Fe_BMb(Fe^{II}) variants, resulting in Zn^{II}-Fe_BMb(Fe^{II}), Fe^{II}-Fe_BMb(Fe^{II}) and Cu^{I}-Fe_BMb(Fe^{II}) respectively (see Supplementary methods for more information on the protocol of preparation). The incorporation of the nonheme metal ion into E-Fe_BMb(Fe^{II}) was monitored by UV-vis absorption spectroscopy (Fig. 1d, Supplementary Fig. S2). The binding of the nonheme metal close to the heme center resulted in a shift in the heme Soret band from 432 nm to 433 nm and a split of the 557 nm peak into two shallow bands at 550 nm and 572 nm. An ideal system to probe the role of the nonheme metal ion requires that all structural features, including the nonheme metal coordination sphere and metal-metal distances remain the same, with the only difference being the identity of the nonheme metal ion. To confirm that this is indeed the case, we obtained crystal structures of the three Fe_BMb variants[25] (Fig. 1a–c). A comparison of these structures show that the respective nonheme metal ion in each variant is coordinated to three histidines (H64, H43, H29) and a glutamate (68E) in a distorted trigonal-bipyramidal geometry, thereby conserving the desired coordination sphere. Furthermore, the heme-nonheme metal distances remain the same (~4.5 Å) within the experimental error of the X-ray crystallography resolution (~1.7 Å). In all, these results confirm that the Fe_BMb variants constitute a model system to probe different nonheme metals within the same protein scaffold, and holds potential to elucidate the preference for copper exhibited by native HCOs.

Armed with such a model system of Fe_BMb variants, we proceed to directly probe the role of nonheme metal on oxidase activity, as measured by the overall oxygen reduction rates (k) and the product selectivity (S) (Fig. 1e). S is defined as the ratio of water produced, the desired end product from the full four-electron oxygen reduction process, to products from incomplete oxygen reduction such as peroxide and superoxide, collectively known as reactive oxygen species or ROS. From a biological perspective, the formation of ROS not only decreases the HCO efficiency, but also damages other cellular components. In this study, we measured the overall oxygen reduction rates for various Fe_BMb variants under multi-turnover conditions using an oxygen electrode, with N,N,N',N'-tetramethyl-p-phenylenediamine (TMPD) as a redox mediator, and ascorbate as a reductant, using a protocol reported previously for both native HCOs and their models.[27] A slightly modified approach employing catalase and superoxide dismutase (SOD)[27] was used to determine the product selectivity in these reactions. The oxygen reduction reaction with E-Fe_BMb(Fe^{II}) (18 μM) showed an initial rapid decrease in oxygen concentration by an amount corresponding to ~1 molar equivalent of protein concentration, attributable to the binding of O_2 to the heme (Supplementary Fig. S3). This initial rapid decrease was followed by a slow decrease of O_2 concentration, with an initial rate of 0.21 (± 0.03) μM/s, of which only ~59% of O_2 was converted to water while the rest was reduced to ROS. The oxygen reduction rates and product selectivity for the Zn^{II}-Fe_BMb(Fe^{II}) (k=0.22(± 0.02), S = 57%) are similar to those of E-Fe_BMb(Fe^{II}). In contrast, both Fe^{II}- and Cu^{I}-Fe_BMb(Fe^{II}) variants showed dramatic enhancements in oxygen reduction rates and product selectivity (k= 1.15 ± 0.07 μM/s and S = 96% for Fe, and k = 2.72 ± 0.1 μM/s and S=94% for Cu). More specifically, the oxidase activity, defined as the rate of water production, of Fe^{II}-Fe_BMb(Fe^{II}) and Cu^{I}-Fe_BMb(Fe^{II}) were 11-fold and 30-fold higher, respectively, than that of Zn^{II}-Fe_BMb(Fe^{II}).

We also note that controls with wild-type myoglobin (WTMb, without the engineered Fe_B center) and in the presence of Zn^{II}, Fe^{II} and Cu^{I} ions showed similar water production rates as E-Fe_BMb(Fe^{II}), but with a high excess of undesirable ROS production[28] (Supplementary Fig. S4), further confirming that enhancements in oxidase activity occur only when Fe^{II} and Cu^{I} are coordinated to the nonheme Fe_B center. The significantly higher oxidase activity of Fe_BMb variants containing redox-active nonheme metal ions (Fe and Cu) than that containing the redox-inactive Zn strongly suggest that the redox activity of the nonheme metals plays a key role in oxygen reduction, probably by donating electrons to complete the four-electron reduction of oxygen to water. To support this hypothesis, we used electron paramagnetic resonance (EPR) and X-ray near edge (XANES) spectroscopy to monitor oxidation state changes of nonheme metal ions when Cu^{I}- and Fe^{II}-Fe_BMb(Fe^{II}) react with oxygen under single-turnover conditions. As shown in Supplementary Fig. S5, both nonheme Cu^{I} and Fe^{II} were oxidized to Cu^{II} and Fe^{III}, suggesting that they donated an electron to oxygen in the process. These spectroscopic experiments in combination with the activity assays not only suggest that the nonheme metal ion acts as an electron donor to oxygen but also reveals the superior performance of Cu over Fe for oxygen reduction reaction.

To investigate reasons behind Nature's choice of copper in HCO's, we first measured the effect of the nonheme metal on heme Fe^{III}/Fe^{II} redox potentials. Spectroelectrochemical[29–30] measurements of the heme redox potential (E°') of E-Fe_BMb showed a value of −159 ± 5 mV. Under the same conditions, the Zn^{II}-, Fe^{II}-, and Cu^{I}-Fe_BMb variants displayed heme E°' values of −45 ± 2 mV, −58 ± 3 mV, −64 ± 4 mV, respectively (Fig. 2a). Because the addition of all three metal ions resulted in a similar shift of heme E°', we conclude that nature of the nonheme metal has little impact on the heme E°' and is not the reason behind observed trends in oxidase activity of Fe_BMb variants. We next employed cyclic voltammetry (CV) to measure the E°' of the nonheme Fe^{III}/Fe^{II} or Cu^{II}/Cu^{I} redox couples at the Fe_B site. Since the CV signals from redox-active heme iron could interfere with those of the nonheme metal, we replaced heme with redox-inactive Zn protoporphyrin to obtain Fe_BMb(Zn^{II}) using a previously reported protocol.[31] The titration of Fe^{II} and Cu^{I} metals into the Fe_B center of Fe_BMb(Zn^{II}) resulted in similar changes in the Soret and visible bands of the UV-Vis spectra, suggesting similar coordination environments of nonheme Fe^{II} and Cu^{I} in Fe_BMb(Zn^{II}) (Supplementary Fig. S6). The CV experiments conducted on Fe^{II}-Fe_BMb(Zn^{II}) and Cu^{I}-Fe_BMb(Zn^{II}) showed a single, reversible redox transition corresponding to an E°' value of +259 ± 20 mV and +387 ± 25 mV for nonheme Fe^{III}/Fe^{II} or Cu^{II}/Cu^{I} redox couples, respectively (Fig. 2b and c). The E°' values of nonheme metals measured in these experiments are consistent with those reported in literature for nonheme Fe in *c*NOR (~ +300 mV)[32] and for Cu in HCOs (+350 to +400 mV).[3,33–34] Therefore, we conclude that the higher E°' of copper as compared to iron at the nonheme site can provide higher driving force for faster electron transfer to the heterobinuclear catalytic center. Electron transfer to Fe_BMb variants is a rate-determining factor for oxygen reduction reaction: increasing the concentration of electron donor (TMPD/ascorbate) increases the oxygen reduction rate for both Cu^{I}-Fe_BMb(Fe^{II}) and Fe^{II}-Fe_BMb(Fe^{II}) (Supplementary Fig. S7). The higher E°' of copper as compared to iron helps Cu-Fe_BMb achieve faster electron transfer as compared to Fe-Fe_BMb, and thus is an important contributor to enhanced oxidase

activity of Cu-Fe_BMb. While these results clearly indicate that high E°' and thus the driving force of electron transfer play a key role in making Cu a better choice for oxidase activity, we cannot rule out that the reorganization energy difference between Cu and Fe may also play a role.

Having probed the roles of E°'s on the oxidase activity, we move on to understand their interaction with oxygen at the catalytic center *via* stopped-flow UV-Vis absorption spectroscopy under single turnover conditions. The reaction of the reduced E-Fe_BMb(Fe^{II}) with O_2 showed a clean transition from ferrous heme to heme-oxy complex with a Soret blue shift from 432 nm to 414 nm and well-defined visible absorption bands at 541 and 578 nm, typical of heme(Fe^{II})-O_2 complexes[35–38] (Fig. 2d). A similar spectral transition (Fig. 2e) was observed on reacting Zn^{II}-Fe_BMb(Fe^{II}) with O_2, indicating the formation of a stable heme-oxy complex in the Zn-bound Fe_BMb variant. On the other hand, clear formation of heme-oxy was not observed in the case of the Fe^{II}- and Cu^{I}- bound Fe_BMb(Fe^{II}) variants, as the redox active nonheme metals donate electrons to the bound oxygen. This electron donation from nonheme metals (Cu and Fe) leads to the formation of highly reactive forms of oxygen (e.g. peroxy) that are difficult to capture and characterize such that the final product of the reaction is ferric-heme (Supplementary Fig. S8). Nevertheless, a comparison between the O-O bond length of the heme-oxy complex for the E- and Zn^{II}-Fe_BMb(Fe^{II}) can provide insights into potential oxygen activation mechanisms that can arise from the presence of a nonheme metal. To probe this effect, we conducted vibrational studies of these heme-oxy complexes using resonance Raman (RR) spectroscopy. The hemeoxy samples were prepared using $^{18}O_2$ and $^{16}O_2$ saturated buffers to identify the iron-O_2 stretching modes ν(Fe-O_2) since the O-O stretching modes are not observed for His-coordinated heme proteins like Mb (see Supplementary methods for more details on RR sample preparation and data collection).[39] The heme-oxy complex of E-Fe_BMb(Fe^{II}) showed a ν(Fe-O_2) of 575 (−25) cm^{-1} that is typical of heme-oxy species in myoglobin mutants[39–40] (Fig. 2f). In contrast, the heme-oxy complex of Zn^{II}-Fe_BMb(Fe^{II}) showed a much higher ν(Fe-O_2) of 594 (−28) cm^{-1}, suggesting a stronger Fe-O bond and weaker O-O bond as compared to E-Fe_BMb(Fe^{II}). These results suggest that the presence of a nonheme metal like Zn^{II} close to the heme center activates the heme-bound oxygen and weakens its O-O bond.

The RR studies on oxygen added Fe_BMbs show that the nonheme metal ion plays an important role in activating heme-bound oxygen. To further probe this effect and explore whether the extent of oxygen activation was dependent on the identity of the metal ion, we utilized density functional theory (DFT). In these calculations, we modeled the structures of Zn^{II}-, Fe^{II}- and Cu-$^{I}Fe_B$Mb(Fe^{II}) up to the C-alpha (Cα) of each residue to match the crystal structure (refer Fig. 1a–c) for the respective protein systems. The O_2 molecule was then added, and the resulting structures were optimized to their lowest energy form (refer Supplementary methods for additional details). While the nonheme Zn and Fe retained its ligands (i.e., three histidines and one glutamate) (Fig. 1f and g, respectively), the Cu lost the His64 ligand adopting a square planar geometry similar to the DFT simulated structure of native HCO[41] (Fig. 1h). In all of the optimized molecular structures, the heme Fe was oxidized to its ferric state with an electron transferred to O_2. The Zn-Fe_BMb structure stabilized O_2 as O_2^- such that the distal oxygen could interact with Zn^{II} at the nonheme site. Consistent with the RR studies, the computed O-O bond length of the Zn^{II}- variant (1.298 Å)

was elongated compared to O_2-bound E-Fe_BMb (1.277 Å). On the other hand, the lowest energy form for Fe- and Cu-Fe_BMb variants were found to be O_2^{2-}, further supporting the role of nonheme Fe and Cu as an electron donor to oxygen. These results are consistent with EPR/XANES experiments that suggest the oxidation of nonheme metals (Fe and Cu) on their interaction with oxygen. Moreover, the O-O bond length was found be even longer in the Fe^{III}-Fe_BMb(Fe^{III}) variant (1.351 Å), and the longest in the Cu^{II}-Fe_BMb(Fe^{III}) (1.391 Å).These studies demonstrate highly enhanced activation of O_2, both in terms of charge and O-O bond length, with Cu as the nonheme metal, as compared to Fe (Table 1). This can be attributed to the *d*-electron configuration of Cu^{II} (d^9) as compared to Fe^{III} (d^5), that enables Cu to push a higher degree of *d*-electron density to the HOMO orbital of O_2 *via* $d\pi$-$p\pi$ back bonding. Together, these studies further confirm the functional and chemical preference for copper over iron as the nonheme metal in HCOs.

Conclusion

The reduction of oxygen to water requires fast and concomitant electron transfer as well as efficient O-O bond cleavage.[42–43] Our results show that copper is superior to iron in promoting both faster electron transfer by possessing a higher E°' and thus, driving force for electron transfer, as well as weakening of the O-O bond, making it an appropriate choice as the nonheme metal in HCOs. In fact, a comparison of copper with other *3d* transition metals suggest that it's the only metal in the group that is both redox active and contains the maximum number of *d* electrons for O-O bond activation. This direct comparison of the effect of Cu and Fe in promoting O_2 reduction in the same protein scaffold with otherwise identical active site has allowed us to provide direct evidence for why Nature prefers Cu over Fe in oxidase activity and reasons behind such a choice. By providing functional basis for the choice of copper (over iron) in HCOs, these results also attempt to address important questions in the field of evolutionary biology regarding the biochemical changes that occurred as earth's anaerobic atmosphere became oxygen-rich.[44] We also anticipate our work to be a starting point for more focused efforts directed towards understanding Nature's choice of specific metal ions for various biochemical reactions that can aid the design of novel catalysts required in alternative energy technologies and other industrial applications.

Methods

Preparation of Fe_BMb variants

The nonheme metal bound Fe_BMb variants were prepared as described previously with slight modifications.[24–25] Briefly, E-Fe_BMb(Fe^{III}) was degassed and transferred in anaerobic glovebag, where it was reduced using dithionite and exchanged with a PD10 column equilibrated with 50 mM pH 7.3 Bis-TRIS buffer. $ZnCl_2$, $FeCl_2$ and tetrakis(acetonitrile)Cu(I)hexafluorophosphate were then titrated in the E-Fe_BMb(Fe^{II}) to obtain Zn^{II}-,Fe^{II}- and Cu^{I}-Fe_BMb(Fe^{II}) variants respectively.

Oxygen consumption assays

The rate of water and ROS production was measured and calculated as reported previously[27,29,45] with slight modifications. The oxygen consumption assay was initiated by

the addition of 18 μM of metal-bound Fe_BMb to 18 mM ascorbate and 1.8 mM of TMPD/ascorbate incubated in air saturated 100 mM phosphate buffer at pH 6. To calculate the percentage of water with respect to ROS formation, we repeated the measurement of O_2 reduction in the presence of catalase (7 μM) and superoxide dismutase (250 units), which selectively reacts with H_2O_2 and O_2^- to produce O_2. By comparing the rates of reduction in the absence of and in the presence of catalase/SOD, the portion of O_2 reduction that is due to H_2O formation was calculated.

Electrochemistry

The heme E°' was measured by a spectroelectrochemical method using an optically transparent thin-layer cell and the analysis of the data was performed as described previously.[29] The E°' of the nonheme metal in $Fe_BMb(Zn^{II})$ was measured by CV experiments as described previously.[46] The Cu^I- and Fe^{II}- incorporated $Fe_BMb(Zn^{II})$ variants were drop-cast onto pyrolytic graphite electrodes and subjected to a potential sweep from −200 mV to 800 mV v/s Ag/AgCl electrode in 50 mM phosphate buffer at pH6 containing 100 mM $NaNO_3$. All measurements were performed using Ag/AgCl as the reference electrode which was calibrated against SHE. All E°' values are reported in the manuscript against SHE.

Stopped-flow kinetic measurements

Experiments were performed on an Applied Photophysics Ltd. (Leatherhead, U.K.) SX18.MV stopped-flow spectrometer equipped with a 256 element photodiode array detector. Two-syringe mixing was employed to mix equal volumes of Fe_BMb variants with oxygen saturated solutions at 8°C. All reported data sets originally consisted of 200 spectra collected over 30 s using logarithmic sampling.

RR sample preparation and data collection

The oxy-Fe_BMb variants were obtained by mixing solutions of 0.6 mM deoxy-Fe_BMbs in 50 mM Bis-TRIS, pH 7.0 with $^{16}O_2$ or $^{18}O_2$-saturated buffer solutions and rapid freezing in liquid ethane at −120 °C to quench the reaction in the millisecond to second timescale. The RR spectra were obtained on samples maintained at 110 K using a 407 nm excitation from a Kr laser (Innova 302C, Coherent) and a custom McPherson 2061/207 spectrograph equipped with a liquid-nitrogen cooled CCD detector (LN-1100PB, Princeton Instruments).

DFT calculations

The O_2 bound HCO models including E-Fe_BMb-O_2, Zn-Fe_BMb-O_2, Fe-Fe_BMb-O_2, and Cu-Fe_BMb-O_2 were studied computationally using the DFT method B3LYP with 6-311G* for all heavy atoms and 6-31G* for hydrogens, which is similar to the ones reported previously for heme and non-heme and copper protein model studies.[47–49] The initial structural models were built from the following X-ray structures with PDB files 3M38, 3M3B, 3M39, and 3M3A respectively. All first coordination shell residues are included in the models and the residues were truncated to Cα positions. The heme substituents were replaced with hydrogens. The labile water ligand in the original X-ray structures of Fe-Fe_BMb and Cu-Fe_BMb were allowed to be displaced by the incoming O_2 ligand. All models were subject to

partial geometry optimizations with only protein residue Cα atoms fixed at the X-ray structure positions to mimic the protein environment, based on the previous work.[50] In the initial setup for Zn-Fe_BMb-O_2, heme iron and O_2 moiety are of Fe^{III}(S=1/2) anti-ferromagnetically coupled with O_2^- (S= −1/2). In case where the second metal is Fe and Cu, the initial set up of non-heme site metal is in its oxidized state (i.e. Fe^{III} and Cu^{II}) with O_2 being set up as peroxide. Both ferromagnetic and antiferromagnetic coupling modes between this site and heme iron were studied. In addition to the electronic energy (E), the zero-point energy corrected electronic energy (E_{ZPE}), and the enthalpy and Gibbs free energies at the ambient conditions were also calculated in each case. All calculations were performed using the Gaussian 09 program.

More information on experimental design, protocols and data analysis are provided in the supplementary information.

Supplementary Material

Refer to Web version on PubMed Central for supplementary material.

Acknowledgement

We thank Anoop R. Damodaran and Robert B. Gennis for helpful comments and critics on the manuscript. We also thank Parisa Hosseinzadeh, Madeline R. Sponholtz and Sudharsan Dwaraknath for help with various aspects of data collection and analysis. We thank Stanford Synchrotron Radiation Lightsource and Stanford Linear Accelerator for use of their facilities. This material is based upon work supported by the U.S. National Institutes of Health under Award NIH R01GM06211 (to Y.L.), NIH R01GM074785 (to P.M.L.) and U.S. National Science Foundation Award NSF CHE-1300912 (to Y.Z.).

References

1. Ferguson-Miller S, Babcock GT. Heme/copper terminal oxidases. Chem. Rev. 1996; 96:2889–907. [PubMed: 11848844]
2. Namslauer A, Brzezinski P. Structural elements involved in electron-coupled proton transfer in cytochrome *c* oxidase. FEBS Lett. 2004; 567:103–10. [PubMed: 15165901]
3. Kaila VRI, Verkhovsky MI, Wikström M. Proton-coupled electron transfer in cytochrome oxidase. Chem. Rev. 2010; 110:7062–81. [PubMed: 21053971]
4. Wikström M. Cytochrome *c* oxidase: 25 years of the elusive proton pump. Biochim. Biophys. Acta. 2004; 1655:241–47. [PubMed: 15100038]
5. Zumft WG. Nitric oxide reductases of prokaryotes with emphasis on the respiratory, heme-copper oxidase type. J. Inorg. Biochem. 2005; 99:194–215. [PubMed: 15598502]
6. Castresana J, Saraste M. Evolution of energetic metabolism: The respiration-early hypothesis. Trends Biochem. Sci. 1995; 20:443–48. [PubMed: 8578586]
7. Sousa FL, et al. The superfamily of heme-copper oxygen reductases: Types and evolutionary considerations. Biochim. Biophys. Acta, Bioenerg. 2012; 1817:629–37.
8. Sousa FL, et al. Early bioenergetic evolution. Phil. Trans. R. Soc. B. 2013; 368:1–30.
9. Flock U, Watmough NJ, Ädelroth P. Electron/proton coupling in bacterial nitric oxide reductase during reduction of oxygen. Biochemistry. 2005; 44:10711–19. [PubMed: 16060680]
10. Brzezinski P, Gennis RB. Cytochrome *c* oxidase: Exciting progress and remaining mysteries. J. Bioenerg. Biomembr. 2008; 40:521–31. [PubMed: 18975062]
11. Konstantinov AA. Cytochrome c oxidase: Intermediates of the catalytic cycle and their energy-coupled interconversion. FEBS Lett. 2012; 586:630–39. [PubMed: 21889506]
12. Kim E, Chufan EE, Kamaraj K, Karlin KD. Synthetic models for heme-copper oxidases. Chem. Rev. 2004; 104:1077–1133. [PubMed: 14871150]

13. Collman JP, Ghosh S. Recent applications of a synthetic model of cytochrome c oxidase: Beyond functional modeling. Inorg. Chem. 2010; 49:5798–5810. [PubMed: 20527796]
14. Hematian S, Garcia-Bosch I, Karlin KD. Synthetic heme/copper assemblies: Toward an understanding of cytochrome c oxidase interactions with dioxygen and nitrogen oxide. Acc. Chem. Res. 2015; 48:2462–74. [PubMed: 26244814]
15. Collman JP, Dey A, Yang Y, Ghosh S, Decreau RA. O2 reduction by a functional heme/nonheme bis-iron NOR model complex. Proc. Natl. Acad. Sci. U. S. A. 2009; 106:10528–33. [PubMed: 19541624]
16. Raven EL. Designer haem proteins: What can we learn from protein engineering? Heteroat. Chem. 2002; 13:501–05.
17. Gibney BR, Tommos C. De novo protein design in respiration and photosynthesis. Adv. Photosynth. Respir. 2005; 22:729–51.
18. Korendovych IV, et al. Design of a switchable eliminase. Proc. Natl. Acad. Sci. U. S. A. 2011; 108:6823–27. [PubMed: 21482808]
19. Gibney, BR. Metallopeptides as tools to understand metalloprotein folding and stability. Taylor & Francis; 2011. p. 227-45.
20. Zastrow ML, Pecoraro VL. Designing functional metalloproteins: From structural to catalytic metal sites. Coord. Chem. Rev. 2013
21. Yu F, et al. Protein design: Toward functional metalloenzymes. Chem. Rev. 2014; 114:3495–578. [PubMed: 24661096]
22. Rufo CM, et al. Short peptides self-assemble to produce catalytic amyloids. Nature Chem. 2014; 6:303–9. [PubMed: 24651196]
23. Sigman JA, Kwok BC, Gengenbach A, Lu Y. Design and creation of a Cu(II)-binding site in cytochrome *c* peroxidase that mimics the Cu_B-heme center in terminal oxidases. J. Am. Chem. Soc. 1999; 121:8949–50.
24. Yeung N, et al. Rational design of a structural and functional nitric oxide reductase. Nature. 2009; 462:1079–82. [PubMed: 19940850]
25. Lin Y-W, et al. Roles of glutamates and metal ions in a rationally designed nitric oxide reductase based on myoglobin. Proc. Natl. Acad. Sci. U. S. A. 2010; 107:8581–6. [PubMed: 20421510]
26. Chakraborty S, et al. Recent advances in biosynthetic modeling of nitric oxide reductases and insights gained from nuclear resonance vibrational and other spectroscopic studies. Inorg. Chem. 2015; 54:9317–29. [PubMed: 26274098]
27. Miner KD, et al. A designed functional metalloenzyme that reduces o_2 to h_2o with over one thousand turnovers. Angew. Chem. Intl. Ed. 2012; 51:5589–92.
28. Brantley RE Jr. Smerdon SJ, Wilkinson AJ, Singleton EW, Olson JS. The mechanism of autooxidation of myoglobin. J. Biol. Chem. 1993; 268:6995–7010. [PubMed: 8463233]
29. Bhagi-Damodaran A, Petrik ID, Marshall NM, Robinson H, Lu Y. Systematic tuning of heme redox potentials and its effects on O_2 reduction rates in a designed oxidase in myoglobin. J. Am. Chem. Soc. 2014; 136:11882–85. [PubMed: 25076049]
30. Reedy CJ, Gibney BR. Heme protein assemblies. Chem. Rev. 2004; 104:617–49. [PubMed: 14871137]
31. Chakraborty S, et al. Spectroscopic and computational study of a nonheme iron nitrosyl center in a biosynthetic model of nitric oxide reductase. Angew. Chem. Intl. Ed. 2014; 126:2449–53.
32. Butland G, Spiro S, Watmough NJ, Richardson DJ. Two conserved glutamates in the bacterial nitric oxide reductase are essential for activity but not assembly of the enzyme. J. Bacteriol. 2001; 183:189–99. [PubMed: 11114916]
33. Bolgiano B, Salmon I, Ingledew WJ, Poole RK. Redox analysis of the cytochrome o-type quinol oxidase complex of escherichia coli reveals three redox components. Biochem. J. 1991; 274:723–30. [PubMed: 1849404]
34. Ellis WR, Wang H, Blair DF, Gray HB, Chan SI. Spectroelectrochemical study of the cytochrome *a* site in carbon monoxide inhibited cytochrome *c* oxidase. Biochem. 1986; 25:161–67. [PubMed: 3006749]

35. Ibrahim M, Denisov IG, Makris TM, Kincaid JR, Sligar SG. Resonance raman spectroscopic studies of hydroperoxo-myoglobin at cryogenic temperatures. J. Am. Chem. Soc. 2003; 125:13714–18. [PubMed: 14599210]
36. Chen H, Ikeda-Saito M, Shaik S. Nature of the Fe-O_2 bonding in oxy-myoglobin: Effect of the protein. J. Am. Chem. Soc. 2008; 130:14778–90. [PubMed: 18847206]
37. Unno M, Chen H, Kusama S, Shaik S, Ikeda-Saito M. Structural characterization of the fleeting ferric peroxo species in myoglobin: Experiment and theory. J. Am. Chem. Soc. 2007; 129:13394–5. [PubMed: 17929929]
38. Garcia-Serres R, et al. Distinct reaction pathways followed upon reduction of oxy-heme oxygenase and oxy-myoglobin as characterized by moessbauer spectroscopy. J. Am. Chem. Soc. 2007; 129:1402–12. [PubMed: 17263425]
39. Spiro TG, Soldatova AV, Balakrishnan G. CO, NO and O_2 as vibrational probes of heme protein interactions. Coord. Chem. Rev. 2013; 257:511–27. [PubMed: 23471138]
40. Raven EL, Mauk AG. Chemical reactivity of the active site of myoglobin. Adv. Inorg. Chem. 2001; 51:1–49.
41. Noodleman L, Han Du W-G, Fee JA, Gotz AW, Walker RC. Linking chemical electron-proton transfer to proton pumping in cytochrome c oxidase: Broken-symmetry DFT exploration of intermediates along the catalytic reaction pathway of the iron-copper dinuclear complex. Inorg. Chem. 2014; 53:6458–72. [PubMed: 24960612]
42. Babcock GT, Varotsis C, Zhang Y. Oxygen activation in cytochrome oxidase and in other heme proteins. Biochim. Biophys. Acta. 1992; 1101:192–94. [PubMed: 1321667]
43. Babcock GT. How oxygen is activated and reduced in respiration. Proc. Natl. Acad. Sci. U. S. A. 1999; 96:12971–73. [PubMed: 10557256]
44. Saraste M, Castresana J. Cytochrome oxidase evolved by tinkering with denitrification enzymes. FEBS Letters. 1994; 341:1–4. [PubMed: 8137905]
45. Liu X, et al. Significant increase of oxidase activity through the genetic incorporation of a tyrosine-histidine cross-link in a myoglobin model of heme-copper oxidase. Angew. Chem. Intl. Ed. 2012; 51:4312–6.
46. Marshall NM, et al. Rationally tuning the reduction potential of a single cupredoxin beyond the natural range. Nature. 2009; 462:113–7. [PubMed: 19890331]
47. Zhang Y, Oldfield E. On the mossbauer spectra of isopenicillin n synthase and a model {FeNO}7 (S = 3/2) system. J. Am. Chem. Soc. 2004; 126:9494–95. [PubMed: 15291525]
48. Zhang Y, Oldfield E. NMR hyperfine shifts in blue copper proteins: A quantum chemical investigation. J. Am. Chem. Soc. 2008; 130:3814–23. [PubMed: 18314973]
49. Ling Y, Zhang Y. Mossbauer, NMR, geometric, and electronic properties in S = 3/2 iron porphyrins. J. Am. Chem. Soc. 2009; 131:6386–88. [PubMed: 19415933]
50. Yang L, Ling Y, Zhang Y. HNO binding in a heme protein: Structures, spectroscopic properties, and stabilities. J. Am. Chem. Soc. 2011; 133:13814–17. [PubMed: 21834502]

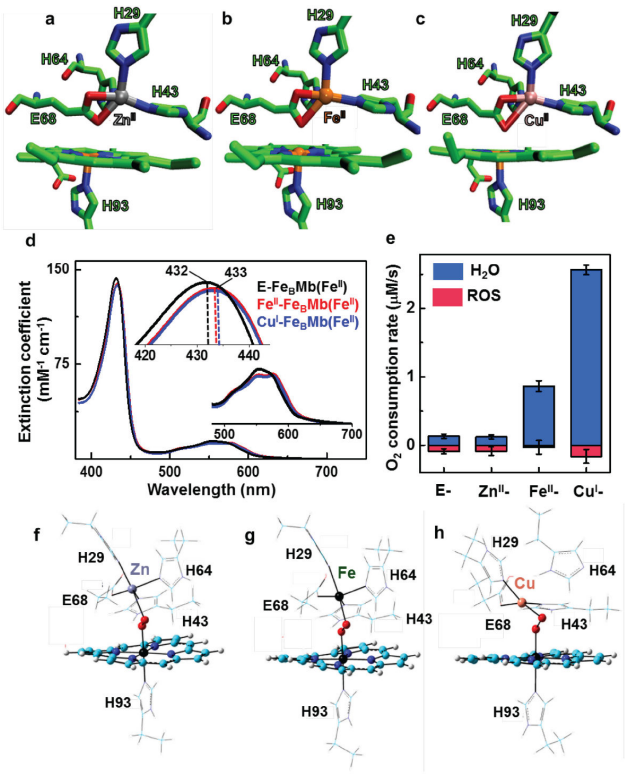

Figure 1. Structure and function of Fe_BMb variants

Crystal structure of Fe_BMb mutant (I107E-Fe_BMb) showing the catalytic heme-nonheme heterobinuclear metal center with Zn^{II} (a, PDB: 3M3B), Fe^{II} (b, PDB: 3M39) and Cu^{II} (c, PDB: 3M3A) nonheme metal ions bound. The heme and amino acid residues as shown in licorice while the nonheme metal ions are shown in VDW representation as a sphere. (d) The UV-Vis spectroscopic measurements on $Fe_BMb(Fe^{II})$ variants displaying the changes in the Soret (420–445 nm) and visible (500–700 nm) region on incorporation of nonheme Fe^{II} and Cu^{I} metal ions. (e) The rates of O_2 reduction to form either H_2O (blue) or ROS (red) catalyzed by 18 μM $Fe_BMb(Fe^{II})$ variants in 100 mM phosphate buffer (pH 6) containing ~0.25 mM O_2, 1.8 mM TMPD, and 18 mM ascorbate. Error bars indicate standard deviation. (f) The DFT-optimized structure of O_2-added Zn- (a), Fe- (b) and Cu-Fe_BMb (c). The porphyrin is shown in licorice while the oxygen molecule and metal ions are shown as sphere.

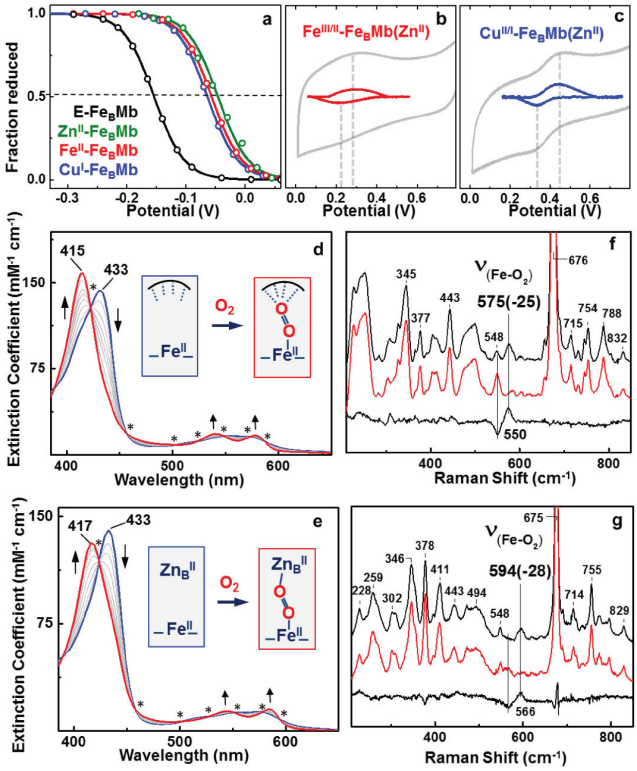

Figure 2. Electrochemical, spectroscopic and kinetic investigation of Fe_BMb variants

(a) Nernst fit of the spectral plot for Fe_BMb(Fe^{II}) and its variants. Dotted lines represent the point where fraction of protein reduced is equal to that oxidized and the corresponding value is the heme E°'. (b) Cyclic voltammogram of Fe^{II}- and (c) Cu^{I}- incorporated Fe_BMb(Zn^{II}). The experimental data is shown in grey while the baseline corrected data is shown in red and blue for Fe- and Cu- respectively. The dotted lines show the midpoint of reduction and oxidation wave. Data exceeding 0.8 V has not be shown as water oxidation catalytic wave begins to appear. Error in the E°' values indicate standard deviation. The stopped-flow UV-Vis measurements of the reaction between 10 μM of E-Fe_BMb(Fe^{II}) (d) and Zn^{II}-Fe_BMb(Fe^{II}) (e) and O_2 saturated buffer between 0.001s to 0.8s. The isosbestic points are represented by a star. The intermediate spectra are shown in grey. The inset shows the structures of the starting and the ending species shown *via* blue and red spectra respectively. The dotted lines in the blue species of (d) represent the distal amino acid residues in E-Fe_BMb that are capable of H-bonding to the bound O_2. The low-frequency RR spectra of E-Fe_BMb(Fe^{II})-O_2 (f) and Zn^{II}-Fe_BMb(Fe^{II})-O_2 (g) obtained at 407 nm excitation.

Table 1

Bond length and charge parameters of O_2 added Zn-, Fe- and Cu- Fe_BMb variants. R_{M-O} is the bond length of nonheme metal and distal oxygen, R_{O-O} is the O-O bond length and Q_{O-O} is the charge on oxygen in the optimized structures.

	R_{M-O} (Å)	R_{O-O} (Å)	Q_{O-O} (e)
Zn-	2.34	1.298	−0.528
Fe-	1.96	1.351	−0.773
Cu-	1.91	1.391	−0.917